

Adaptive domain decomposition techniques in electromagnetic field computation and electrothermomechanical coupling problems

R. H. W. Hoppe

Summary. We consider efficient iterative solvers for the numerical solution of systems of PDEs arising in the computation of electromagnetic fields and in electrothermomechanical coupling problems. We focus on domain decomposition methods on nonmatching grids, also known as mortar element methods, and the solution of the resulting saddle point problems by multilevel preconditioned iterative schemes. The underlying hierarchy of triangulations is generated by adaptive grid refinement/coarsening on the basis of efficient and reliable residual type a posteriori error estimators. In particular, with regard to the electromagnetic field computations we rely on the use of edge element discretizations which require an appropriate treatment of the nontrivial kernel of the discrete curl operator by means of a distributed smoothing process. As applications, we address the numerical simulation of the operational behavior of integrated high voltage modules which is strongly determined by the coupling of electrical, thermal, and mechanical phenomena, and the structural optimization of high power electronic devices and systems featuring an all-in-one approach by primal-dual Newton interior-point methods.

1 Introduction

In this paper, we address adaptive nonconforming domain decomposition methods with emphasis on those on nonmatching grids, also known as mortar element methods. This approach was originally introduced within the framework of spectral elements (see [7, 8]) and has been subsequently studied to some extent for conforming P1 elements (cf., e.g., [1, 2, 5, 10] as well as [28] and its references). For mixed finite elements we refer to [22] whereas mortar edge elements have been considered in [6, 16, 25]. Related three-field techniques have been studied in [11].

Mortar element techniques are particularly useful in the case of discontinuously varying coefficients across interior interfaces as, for instance, material interfaces [9, 19] or for moving subdomain interfaces [25] where it would be computationally expensive to achieve conformity of the global discretization. Another application is that of interior-exterior domain problems as they typically arise in electromagnetics [20, 21].

The contents of the paper are as follows. In Sect. 2, we consider domain decomposition methods on nonmatching grids for individual subdomain discretizations both by standard Lagrange finite elements as well as by curl-conforming edge elements (the latter are aimed at the computation of electromagnetic fields or electromagnetic potentials). In both cases, we need to impose weak continuity constraints on the interfaces in order to guarantee consistency of the overall discretization which

will be done by means of Lagrange multipliers in appropriately chosen multiplier spaces. This leads to the solution of saddle point problems that are taken care of by suitable multilevel methods. For adaptive grid refinement, we focus on efficient and reliable residual-type a posteriori error estimators giving rise to extra terms due to the nonconformity on the subdomain interfaces. As far as applications in high performance scientific computing are concerned, we will focus on two technologically relevant problems in high power electronics. The first one, dealt with in Sect. 3, concerns electrothermomechanical coupling effects in integrated high voltage (IHV) modules which are tackled by mortar P1 element methods applied to the underlying thermal and mechanical balance equations. Particular emphasis is on the computation of the von Mises equivalence stresses serving as an indicator for possible material failure (cf. [9, 19]). The other application, considered in Sect. 4, addresses the structural optimization of AC–DC converter modules that are used as electric drives for high power electromotors. Here, we are faced with a topology-optimization problem featuring equality and inequality constraints on the design parameters and the state variables, the latter subject to the eddy currents equations in their potential formulation. We advocate an all-in-one approach by means of primal-dual Newton interior-point methods featuring simultaneous sequential quadratic programming (SQP) where the iterative solution of the discretized state equations is an integral part of the optimization loop (cf. [20, 21]).

2 Domain decomposition on nonmatching grids

We first consider mortar methods for Lagrange finite elements applied to the elliptic boundary value problem

$$Lu := -\operatorname{div}(a \mathbf{grad} u) + cu = f, \quad \text{in } \Omega \subset \mathbf{R}^3, \quad (1)$$

$$\mathbf{n} \cdot a \mathbf{grad} u = g, \quad \text{on } \Gamma_N \subset \Gamma := \partial\Omega, \quad u = 0, \quad \text{on } \Gamma_D := \Gamma \setminus \Gamma_N \quad (2)$$

under the usual assumptions on the data of the problem. The variational formulation is to find $u \in H_{0,\Gamma_D}^1(\Omega) := \{v \in H^1(\Omega) \mid v|_{\Gamma_D} = 0\}$ such that

$$\int_{\Omega} (a \nabla u \cdot \nabla v + cuv) dx = \int_{\Omega} f v dx + \int_{\Gamma_N} g v d\sigma, \quad v \in H_{0,\Gamma_D}^1(\Omega). \quad (3)$$

We start from a nonoverlapping decomposition of Ω into n mutually disjoint subdomains

$$\bar{\Omega} = \bigcup_{i=1}^n \Omega_i, \quad \Omega_i \cap \Omega_j \neq \emptyset, \quad 1 \leq i \neq j \leq n, \quad (4)$$

and we assume the decomposition to be geometrically conforming in the sense that two adjacent subdomains either share a face, an edge, or a vertex. We use individual

simplicial triangulations \mathcal{T}_i of the subdomains Ω_i , $1 \leq i \leq n$, regardless of the situation on the skeleton of the decomposition

$$S := \bigcup_{i \neq j} \Gamma_{ij}, \quad \Gamma_{ij} := \bar{\Omega}_i \cap \bar{\Omega}_j \neq \emptyset \tag{5}$$

composed of the interfaces Γ_{ij} between adjacent subdomains Ω_i and Ω_j where typically nonconforming nodal points will arise. We note that the interfaces Γ_{ij} inherit two different triangulations, namely, \mathcal{T}_{ij} from the triangulation \mathcal{T}_i of Ω_i and \mathcal{T}_{ji} from the triangulation \mathcal{T}_j of Ω_j . We refer to Ω_j as the mortar and to Ω_i as the nonmortar side. Setting $h_k := \min\{\text{diam}(T) \mid T \in \mathcal{T}_k, T \cap \Gamma_{ij} \neq \emptyset\}$, $k = i$ or $k = j$, we assume the existence of positive constants $0 < c \leq C$ such that

$$ch_j \leq h_i \leq Ch_j, \quad \Gamma_{ij} \subset S. \tag{6}$$

We denote by $S_{1,\Gamma_D}(\Omega_i; \mathcal{T}_i)$ the finite element spaces of continuous, piecewise linear finite elements, vanishing on the Dirichlet boundary Γ_D , and consider the product space

$$V_h := \prod_{i=1}^n S_{1,\Gamma_D}(\Omega_i; \mathcal{T}_i) \tag{7}$$

with norm $\|v_h\|_{V_h} := \left(\sum_{i=1}^n \|v_h\|_{1;\Omega_i}^2 \right)^{1/2}$.

It is clear that $V_h \not\subset H_{0,\Gamma_D}^1(\Omega)$ since, due to the occurrence of nonconforming nodal points, we do not have continuity across the interfaces. Therefore, in order to ensure consistency we have to impose continuity constraints. This can be done either by means of Lagrange multipliers in suitably chosen multiplier spaces, thus working in the unconstrained space, or, alternatively, by considering the continuity constraints as part of the trial space which means working in a constrained space. In the latter case, an appropriate basis has to be specified which can be done in terms of a dual basis (see, e.g., [28]).

In what follows, we concentrate on the first approach and work on the unconstrained product space V_h . The multiplier space $M_h(S)$ is constructed by means of the traces on the interfaces Γ_{ij} with respect to the triangulation \mathcal{T}_{ij} inherited from the nonmortar side:

$$M_h(S) := \prod_{\Gamma_{ij}} M_h(\Gamma_{ij}), \tag{8}$$

where $M_h(\Gamma_{ij})$ is chosen such that

$$S_{1,0}(\Gamma_{ij}; \mathcal{T}_{ij}) \subset M_h(\Gamma_{ij}), \quad \dim M_h(\Gamma_{ij}) = \dim S_{1,0}(\Gamma_{ij}; \mathcal{T}_{ij}).$$

$M_h(S)$ will be equipped with an appropriate mesh-dependent norm $\|\cdot\|_{M_h(S)}$ (see, e.g., [10, 28]).

In particular, the construction of $M_h(\Gamma_{ij})$ requires a modification of those nodal basis functions associated with nodal points in Γ_{ij} having neighboring nodal points on the boundary $\partial\Gamma_{ij}$ of Γ_{ij} by adding a convex combination of the respective nodal basis functions associated with nodal points on $\partial\Gamma_{ij}$. In 2D, this simply means that we have constant basis functions at both ends of an interface Γ_{ij} , but the construction is more involved in 3D. We refer to [10] for details.

We denote by $a_h(\cdot, \cdot) : V_h \times V_h \rightarrow \mathbf{R}$ the bilinear form associated with the finite element discretized subdomain problems

$$a_h(\cdot, \cdot) := \sum_{i=1}^n \int_{\Omega_i} (a \nabla u_h \cdot \nabla v_h + c u_h v_h) dx, \quad u_h, v_h \in V_h,$$

by $b_h(\cdot, \cdot) : V_h \times M_h(S) \rightarrow \mathbf{R}$ the bilinear form that realizes the weak continuity constraints across the interfaces

$$b_h(\cdot, \cdot) := - \sum_{\Gamma_{ij} \subset S} \int_{\Gamma_{ij}} [v_h]_J \mu_h d\sigma, \quad v_h \in V_h, \mu_h \in M_h(S),$$

where $[v_h]_J$ denotes the jump of $v_h \in V_h$ across Γ_{ij} , and by $\ell_h(\cdot) : V_h \rightarrow \mathbf{R}$ the functional

$$\ell_h(v_h) := \int_{\Omega} f v_h dx + \int_{\Gamma_N} g v_h d\sigma, \quad v_h \in V_h.$$

Then, the mortar finite element approximation is given by the discrete saddle point problem

$$a_h(u_h, v_h) + b_h(v_h, \lambda_h) = \ell_h(v_h), \quad v_h \in V_h, \tag{9}$$

$$b_h(u_h, \mu_h) = 0, \quad \mu_h \in M_h(S). \tag{10}$$

Denoting by $B_h : V_h \rightarrow M_h(S)^*$ the operator associated with the bilinear form $b_h(\cdot, \cdot)$, we have

Theorem 1 (cf. [5, 10]). *The bilinear form $a_h(\cdot, \cdot)$ is elliptic on $\text{Ker} B_h$, and the bilinear form $b_h(\cdot, \cdot)$ satisfies the inf-sup condition*

$$\inf_{\mu_h \in M_h(S)} \sup_{v_h \in V_h} \frac{b_h(v_h, \mu_h)}{\|v_h\|_{V_h} \|\mu_h\|_{M_h(S)}} \geq \beta > 0. \tag{11}$$

For the iterative solution of the resulting algebraic saddle point problem

$$\mathcal{A} \begin{pmatrix} u \\ \lambda \end{pmatrix} = \begin{pmatrix} A & B^T \\ B & 0 \end{pmatrix} \begin{pmatrix} u \\ \lambda \end{pmatrix} = \begin{pmatrix} b \\ 0 \end{pmatrix} \tag{12}$$

there are several multilevel approaches among which we only mention two: the first is a multilevel preconditioned Lanczos iteration featuring a block diagonal preconditioner

$$\mathcal{R} = \begin{pmatrix} R_u & 0 \\ 0 & R_\lambda \end{pmatrix}. \tag{13}$$

The first diagonal block is a block-diagonal matrix $R_u = \text{diag}(R_1, \dots, R_n)$ where the diagonal blocks R_i , $1 \leq i \leq n$, are the subdomain blocks of the BPX preconditioner which is spectrally equivalent to the subdomain stiffness matrices. The second diagonal block R_λ is spectrally equivalent to the Schur complement $S_\lambda := BA^{-1}B^T$ and can be realized in terms of inner preconditioned Chebyshev iterations involving preconditioners for the local, i.e., subdomain-wise Schur complements (cf., e.g., [12, 18] for details).

An alternative approach is to use a multigrid method featuring a block-preconditioned Richardson-type iteration

$$\begin{pmatrix} u^{k+1} \\ \lambda^{k+1} \end{pmatrix} = \begin{pmatrix} u^k \\ \lambda^k \end{pmatrix} - \begin{pmatrix} R & B^T \\ B & 0 \end{pmatrix}^{-1} \left\{ \begin{pmatrix} A & B^T \\ B & 0 \end{pmatrix} \begin{pmatrix} u^k \\ \lambda^k \end{pmatrix} - \begin{pmatrix} b \\ 0 \end{pmatrix} \right\}$$

both as a smoother and as an iterative solver on the coarsest grid where $R := \text{diag}(R_1, \dots, R_n)$ with R_i , $1 \leq i \leq n$, being Gauss–Seidel sweeps on the discretized subdomain problems. Efficient implementation requires a subtle modification of R by using a non-diagonal preconditioner only for the unknowns associated with the interior of the subdomains (see, e.g., [10] for details).

Local adaptive grid refinement is done by an efficient and reliable residual-type a posteriori error estimator.

Theorem 2 (cf. [12, 18]). *Denoting by $(u_M, \lambda_M) \in V_h \times M_h(S)$ the solution of (9),(10), there exist constants $0 < \gamma_R \leq \Gamma_R$ independent of the refinement level such that*

$$\gamma_R \eta_R^2 \leq \|u - u_M\|_V^2 \leq \Gamma_R \eta_R^2,$$

where

$$\eta_R^2 := \sum_{i=1}^n \sum_{T \in \mathcal{T}_i} \eta_{R;T}^2,$$

$$\begin{aligned} \eta_{R;T}^2 &:= h_T^2 \|f - Lu_M\|_{0;T}^2 + \sum_{F \subset \partial T \cap \Omega_i} h_F \|[\mathbf{n} \cdot a \nabla u_m]_J\|_{0;F}^2 \\ &+ \sum_{\Gamma_{ij} \subset S} \sum_{F \subset \partial T \cap \Gamma_{ij}} h_F \|\mathbf{n} \cdot a \nabla u_M - \lambda_M\|_{0;F}^2 \\ &+ \sum_{\Gamma_{ij} \subset S} \sum_{F \subset \partial T \cap \Gamma_{ij}} h_F^{-1} \|[u_M]_J\|_{0;F}^2. \end{aligned}$$

The local contributions of the estimator essentially consist of two parts, those stemming from the individual discretizations of the subdomain problems (the first two terms on the right-hand side of the equation defining $\eta_{R;T}^2$) and those associated with the interfaces which are a weighted L^2 -norm of the defect in the approximation of the flux by the multiplier λ_M and a weighted L^2 -norm of the jumps of u_M across the

interfaces which is typical for nonconforming approaches (for details see, e.g., [12, 18]).

Next, we give a brief outline of mortar edge element methods applied to the following boundary value problem for the double curl-operator

$$\mathbf{curl} a \mathbf{curl} \mathbf{j} + c\mathbf{j} = \mathbf{f} \quad \text{in } \Omega \subset \mathbf{R}^3, \tag{14}$$

$$\mathbf{n} \wedge \mathbf{j} = 0 \quad \text{on } \Gamma = \partial\Omega, \tag{15}$$

where for simplicity we assume vanishing tangential traces on the boundary Γ . The variational formulation involves the Hilbert space $\mathbf{H}(\mathbf{curl}; \Omega)$ with norm $\|\cdot\|_{\mathbf{curl};\Omega}$ and its subspace $\mathbf{H}_0(\mathbf{curl}; \Omega) := \{\mathbf{q} \in \mathbf{H}_0(\mathbf{curl}; \Omega) \mid \mathbf{n} \wedge \mathbf{q} \mid_{\Gamma} = \mathbf{0}\}$, namely, find $\mathbf{j} \in \mathbf{H}_0(\mathbf{curl}; \Omega)$ such that

$$\int_{\Omega} (a \mathbf{curl} \mathbf{j} \cdot \mathbf{curl} \mathbf{q} + c\mathbf{j} \cdot \mathbf{q}) dx = \int_{\Omega} \mathbf{f} \cdot \mathbf{q} dx, \quad \mathbf{q} \in \mathbf{H}_0(\mathbf{curl}; \Omega). \tag{16}$$

For discretization we use the lowest order curl-conforming edge elements of Nédélec’s first family (cf. [24]). Again, we consider a nonoverlapping geometrically conforming decomposition of Ω according to (4) and individual simplicial triangulations \mathcal{T}_i of Ω_i , $1 \leq i \leq n$. We refer to $Nd_{1,0}(\Omega_i; \mathcal{T}_i)$, $1 \leq i \leq n$, as the corresponding edge element spaces with vanishing tangential traces on Γ and consider the product space

$$V_h := \prod_{i=1}^n Nd_{1,0}(\Omega_i; \mathcal{T}_i) \tag{17}$$

with norm $\|\cdot\|_V := (\sum_{i=1}^n \|\cdot\|_{\mathbf{curl};\Omega_i}^2)^{1/2}$.

Due to nonconforming edges on the interfaces Γ_{ij} between adjacent subdomains, there is a lack of continuity across the interfaces: neither the tangential traces $\mathbf{n} \wedge \mathbf{q}_h$ nor the tangential trace components $\mathbf{n} \wedge (\mathbf{n} \wedge \mathbf{q}_h)$ can be expected to be continuous. Denoting by $\mathbf{Nd}_1(\Gamma_{ij}; \mathcal{T}_{ij})$, resp., $\mathbf{RT}_0(\Gamma_{ij}; \mathcal{T}_{ij})$, the edge element space, resp., the lowest order Raviart–Thomas space, on Γ_{ij} with respect to the triangulation \mathcal{T}_{ij} inherited from the nonmortar side, we note that $(\mathbf{n} \wedge \mathbf{q}_h) \mid_{\Gamma_{ij}} \in \mathbf{RT}_0(\Gamma_{ij}; \mathcal{T}_{ij})$, respectively, $(\mathbf{n} \wedge (\mathbf{n} \wedge \mathbf{q}_h)) \mid_{\Gamma_{ij}} \in \mathbf{Nd}_1(\Gamma_{ij}; \mathcal{T}_{ij})$. Therefore, we may enforce continuity in terms of either the tangential traces or the tangential trace components. For instance, if we choose the tangential traces, the multiplier space $\mathbf{M}_h(\mathbf{S})$ can be constructed according to

$$\mathbf{M}_h(\mathbf{S}) := \prod_{\Gamma_{ij} \subset \mathbf{S}} \mathbf{M}_h(\Gamma_{ij}) \tag{18}$$

with $\mathbf{M}_h(\Gamma_{ij})$ chosen such that

$$\mathbf{RT}_{0,0}(\Gamma_{ij}; \mathcal{T}_{ij}) \subset \mathbf{M}_h(\Gamma_{ij}), \quad \dim \mathbf{M}_h(\Gamma_{ij}) = \dim \mathbf{RT}_{0,0}(\Gamma_{ij}; \mathcal{T}_{ij}).$$

We equip $\mathbf{M}_h(\mathbf{S})$ with a mesh-dependent norm $\|\cdot\|_{\mathbf{M}_h(\mathbf{S})}$. Other choices can be made as well (concerning the construction of $\mathbf{M}_h(\Gamma_{ij})$ see [16, 25] for details).

We refer to $a_h(\cdot, \cdot) : \mathbf{V}_h \times \mathbf{V}_h \rightarrow \mathbf{R}$ and $b_h(\cdot, \cdot) : \mathbf{V}_h \times \mathbf{M}_h(\mathbf{S}) \rightarrow \mathbf{R}$ as the bilinear forms

$$a_h(\mathbf{j}_h, \mathbf{q}_h) := \sum_{i=1}^n \int_{\Omega_i} (a \operatorname{curl} \mathbf{j}_h \cdot \operatorname{curl} \mathbf{q}_h + c \mathbf{j}_h \cdot \mathbf{q}_h) dx, \quad \mathbf{j}_h, \mathbf{q}_h \in \mathbf{V}_h$$

$$b_h(\mathbf{q}_h, \boldsymbol{\mu}_h) := \sum_{\Gamma_{ij} \subset \Gamma_{ij}} \int_{\Gamma_{ij}} [\mathbf{n} \wedge \mathbf{q}_h]_J \cdot \boldsymbol{\mu}_h d\sigma, \quad \mathbf{q}_h \in \mathbf{V}_h, \boldsymbol{\mu}_h \in \mathbf{M}_h(\mathbf{S}).$$

The mortar edge element approximation of (14), (15) then amounts to the solution of the saddle point problem: find $(\mathbf{j}_h, \boldsymbol{\lambda}_h) \in \mathbf{V}_h \times \mathbf{M}_h(\mathbf{S})$ such that

$$a_h(\mathbf{j}_h, \mathbf{q}_h) + b_h(\mathbf{q}_h, \boldsymbol{\lambda}_h) = \int_{\Omega} \mathbf{f} \cdot \mathbf{q}_h, \quad \mathbf{q}_h \in \mathbf{V}_h, \tag{19}$$

$$b_h(\mathbf{j}_h, \boldsymbol{\mu}_h) = 0, \quad \boldsymbol{\mu}_h \in \mathbf{M}_h(\mathbf{S}). \tag{20}$$

Again, we denote by $B_h : \mathbf{V}_h \rightarrow \mathbf{M}_h(\mathbf{S})^*$ the operator associated with $b_h(\cdot, \cdot)$. Then we have the following theorem.

Theorem 3 (cf. [6, 16]). *The bilinear form $a_h(\cdot, \cdot)$ is elliptic on $\operatorname{Ker} B_h$, and the bilinear form $b_h(\cdot, \cdot)$ satisfies the LBB-condition*

$$\inf_{\boldsymbol{\mu}_h \in \mathbf{M}_h(\mathbf{S})} \sup_{\mathbf{q}_h \in \mathbf{V}_h} \frac{b_h(\mathbf{q}_h, \boldsymbol{\mu}_h)}{\|\mathbf{q}_h\|_{\mathbf{V}_h} \|\boldsymbol{\mu}_h\|_{\mathbf{M}_h(\mathbf{S})}} \geq \beta > 0. \tag{21}$$

For the numerical solution of the resulting algebraic saddle point problem, the non-trivial kernel of the discrete curl-operator has to be taken into account which is subdomain-wise given by the subspace of irrotational vector fields spanned by the gradients of the finite element functions in $S_{1,0}(\Omega_i; \mathcal{T}_i)$, $1 \leq i \leq n$. Within a multi-level framework, an appropriate way to cope with the nontrivial kernel is to perform a hybrid smoothing process featuring Gauss–Seidel sweeps on the edge element discretized problems followed by a defect correction on the subspaces of irrotational vector fields realized by associated Gauss–Seidel sweeps (cf., e.g., [3, 13]).

In the framework of domain decomposition methods on nonmatching grids, we may adopt this approach, but have to take into account that the defect correction has to be carried out with regard to mortar Lagrange finite element techniques as described in the first part of this section. In more detail, the hybrid smoothing process consists of the following steps.

Step 1. Smoothing on the fully edge element discretized problem.

$$\begin{pmatrix} \mathbf{j}_h^{\mathbf{k}+1} \\ \boldsymbol{\lambda}_h^{\mathbf{k}+1} \end{pmatrix} = \begin{pmatrix} \mathbf{j}_h^{\mathbf{k}} \\ \boldsymbol{\lambda}_h^{\mathbf{k}} \end{pmatrix} - \begin{pmatrix} R_1 & B_1^T \\ B_1 & 0 \end{pmatrix}^{-1} \left\{ \begin{pmatrix} A_1 & B_1^T \\ B_1 & 0 \end{pmatrix} \begin{pmatrix} \mathbf{j}_h^{\mathbf{k}} \\ \boldsymbol{\lambda}_h^{\mathbf{k}} \end{pmatrix} - \begin{pmatrix} \mathbf{b} \\ \mathbf{0} \end{pmatrix} \right\},$$

where $R_1 := \operatorname{diag}(R_1^{(1)}, \dots, R_1^{(n)})$ and $R_1^{(i)}$, $1 \leq i \leq n$, are Gauss–Seidel sweeps on the subdomain problems

$$\int_{\Omega_i} (a \operatorname{curl} \mathbf{j}_h \cdot \operatorname{curl} \mathbf{q}_h + c \mathbf{j}_h \cdot \mathbf{q}_h) dx = \int_{\Omega_i} \mathbf{f} \cdot \mathbf{q}_h dx, \quad \mathbf{q}_h \in Nd_{1,0}(\Omega_i; \mathcal{T}_i).$$

Step 2. Defect correction on the irrotational part.

$$\begin{pmatrix} \varphi_h^{k+1} \\ \eta_h^{k+1} \end{pmatrix} = \begin{pmatrix} \varphi_h^k \\ \eta_h^k \end{pmatrix} - \begin{pmatrix} R_2 & B_2^T \\ B_2 & 0 \end{pmatrix}^{-1} \left\{ \begin{pmatrix} A_2 & B_2^T \\ B_2 & 0 \end{pmatrix} \begin{pmatrix} \varphi_h^k \\ \eta_h^k \end{pmatrix} - \begin{pmatrix} r \\ 0 \end{pmatrix} \right\},$$

where $R_2 := \text{diag}(R_2^{(1)}, \dots, R_2^{(n)})$ and $R_2^{(i)}, 1 \leq i \leq n$, are Gauss–Seidel sweeps on

$$\int_{\Omega_i} c \mathbf{grad} \varphi_h \cdot \mathbf{grad} v_h dx = r(v_h), \quad v_h \in S_{1,0}(\Omega_i; \mathcal{T}_i),$$

where the right-hand side represents the residual

$$r(v_h) := \int_{\Omega_i} \mathbf{f} \cdot \mathbf{grad} v_h dx - a_h|_{\Omega_i}(\mathbf{j}_h, \mathbf{grad} v_h).$$

Step 3. Additive correction.

Denoting by \mathbf{j}_h and φ_h the results of the smoothing Steps 1 and 2, we lastly compute

$$\mathbf{j}_h^{\text{new}} := \mathbf{j}_h + \mathbf{grad} \varphi_h.$$

Again, in both Steps 1 and 2 we use a nondiagonal preconditioner only for the unknowns associated with edges, resp., grid points, in the interior of the subdomains, but a diagonal preconditioner on the skeleton.

The idea behind residual-type a posteriori error estimation in the context of edge element discretizations is to consider the Helmholtz decomposition

$$H_0(\mathbf{curl}; \Omega) = H_0^0(\mathbf{curl}; \Omega) \oplus H_0^\perp(\mathbf{curl}; \Omega)$$

into the subspace $H_0^0(\mathbf{curl}; \Omega)$ of irrotational vector fields and its orthogonal complement $H_0^\perp(\mathbf{curl}; \Omega)$ representing the subspace of weakly solenoidal vector fields.

Denoting by $(\mathbf{j}_M, \lambda_M) \in \mathbf{V}_h \times \mathbf{M}_h(\mathbf{S})$ the solution of (19), (20), we split the error $\mathbf{j}_e := \mathbf{j} - \mathbf{j}_M$ accordingly, i.e., $\mathbf{j}_e = \mathbf{j}_e^0 + \mathbf{j}_e^\perp$, $\mathbf{j}_e^0 \in H_0^0(\mathbf{curl}; \Omega)$, $\mathbf{j}_e^\perp \in H_0^\perp(\mathbf{curl}; \Omega)$, and estimate \mathbf{j}_e^0 and \mathbf{j}_e^\perp separately.

Theorem 4 (cf. [17]). *There exist constants $0 < \gamma_{IR} \leq \Gamma_{IR}$ and $0 < \gamma_{WS} \leq \Gamma_{WS}$ independent of the refinement level such that*

$$\begin{aligned} \gamma_{IR} \eta_{IR}^2 &\leq \|\mathbf{j}_e^0\|_{0;\Omega}^2 \leq \Gamma_{IR} \eta_{IR}^2, \\ \gamma_{WS} \eta_{WS}^2 &\leq \|\mathbf{j}_e^\perp\|_{\mathbf{V}_h}^2 + h^2 \|\mathbf{j}_e^0\|^2, \quad \|\mathbf{j}_e^\perp\|_{\mathbf{V}_h}^2 \leq \Gamma_{WS} \eta_{WS}^2, \end{aligned}$$

$$\text{where} \quad \eta_{IR}^2 := \sum_{i=1}^n \sum_{T \in \mathcal{T}_i} \eta_{IR;T}^2, \quad \eta_{WS}^2 := \sum_{i=1}^n \sum_{T \in \mathcal{T}_i} \eta_{WS;T}^2,$$

$$\begin{aligned}
 \eta_{IR;T}^2 &:= h_T^2 \|\operatorname{div} \mathbf{c} \mathbf{j} \mathbf{M} - \operatorname{div} \mathbf{f}\|_{0;T}^2 + \sum_{F \subset \partial T \cap \Omega_i} h_F \|[\mathbf{n} \cdot (\mathbf{c} \mathbf{j} \mathbf{M} - \mathbf{f})]_J\|_{0;F}^2 \\
 &+ \sum_{\Gamma_{ij} \subset S} \sum_{F \subset \partial T \cap \Gamma_{ij}} h_F \|\lambda_M - \mathbf{n} \cdot \mathbf{c} \mathbf{j} \mathbf{M}\|_{0;F}^2 \\
 &+ \sum_{\Gamma_{ij} \subset S} \sum_{F \subset \partial T \cap \Gamma_{ij}} h_F^{-1} \|[\mathbf{u}_M]_J\|_{0;F}^2,
 \end{aligned}$$

$$\begin{aligned}
 \eta_{WS;T}^2 &:= h_T^2 \|\mathbf{f} - \operatorname{curl} \mathbf{a} \operatorname{curl} \mathbf{j} \mathbf{M} - \mathbf{c} \mathbf{j} \mathbf{M}\|_{0;T}^2 + \\
 &+ \sum_{F \subset \partial T \cap \Omega_i} h_F \|[\mathbf{n} \wedge (\mathbf{n} \wedge \mathbf{a} \operatorname{curl} \mathbf{j} \mathbf{M})]_J\|_{0;F}^2 \\
 &+ \sum_{\Gamma_{ij} \subset S} \sum_{F \subset \partial T \cap \Gamma_{ij}} h_F \|\lambda_h - \mathbf{n} \wedge (\mathbf{n} \wedge \mathbf{a} \operatorname{curl} \mathbf{j} \mathbf{M})\|_{0;F}^2 \\
 &+ \sum_{\Gamma_{ij} \subset S} \sum_{F \subset \partial T \cap \Gamma_{ij}} h_F^{-1} \|[\mathbf{n} \wedge \mathbf{j} \mathbf{M}]_J\|_{0;F}^2,
 \end{aligned}$$

where u_M in the expression for $\eta_{IR;T}^2$ is such that $\operatorname{grad} u_M$ represents the irrotational part of $\mathbf{j} \mathbf{M}$.

3 Electrothermomechanical coupling effects

As an example for the application of mortar element techniques based on individual P1 approximations of the subdomain problems, we consider the numerical simulation of electrothermomechanical coupling effects in integrated high voltage (IHV) modules.

As shown in Fig. 1, such a module consists of specific semiconductor devices such as insulated gate bipolar transistors (IGBTs) and power diodes that are integrated in

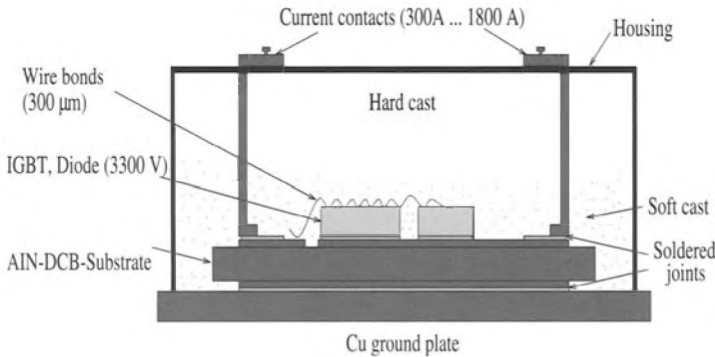


Fig. 1. Integrated high voltage module

copper blocks and connected to current contacts by wire bonds. Due to high currents, up to several kA, there is a considerable self-heating causing thermal stresses that have an impact on the mechanical behavior of the device. To prevent mechanical damage, the blocks are mounted on several layers of different materials attached to each other by thin soldered joints. The ground plate is fixed on a cooling device. Moreover, for electric durability the module is put in a housing filled with soft and hard cast.

The operating behavior of the IHV module can be modelled by a coupled system of PDEs describing the transport processes in the IGBTs and power diodes, the temporal and spatial distribution of the temperature and mechanical deformations due to heat stresses. In particular, the dominant heat source is electrical energy converted to Joule heat

$$H_{\text{Joule}} = \frac{\mathbf{J}_n \cdot \mathbf{J}_n}{q\mu_n n} + \frac{\mathbf{J}_p \cdot \mathbf{J}_p}{q\mu_p p}.$$

Here, n and p are the carrier concentrations, μ_n and μ_p are the mobilities, q is the elementary charge and \mathbf{J}_n and \mathbf{J}_p are the current densities

$$\mathbf{J}_n = -q\mu_n n \nabla \psi, \quad \mathbf{J}_p = -q\mu_p p \nabla \psi$$

with ψ denoting the electric potential. The potential ψ and the current densities \mathbf{J}_n and \mathbf{J}_p can be computed by the drift-diffusion model:

$$-\nabla \cdot \varepsilon \nabla \psi + N_{\text{dop}}(n, p) + q(n - p) = 0, \quad (22)$$

$$\frac{\partial n}{\partial t} = q^{-1} \nabla \cdot \mathbf{J}_n + G(\mathbf{J}_n, \mathbf{J}_p) - R(n, p), \quad (23)$$

$$\frac{\partial p}{\partial t} = -q^{-1} \nabla \cdot \mathbf{J}_p + G(\mathbf{J}_n, \mathbf{J}_p) - R(n, p) \quad (24)$$

with appropriate initial and boundary conditions where N_{dop} refers to the doping profile and G and R stand for the generation and recombination terms (cf., e.g., [23, 26, 27] for the model and [14, 15] for numerical simulations based on mixed hybrid finite element discretizations).

The heat conduction is described by the following initial-boundary value problem for the temperature T :

$$\rho c \frac{\partial T}{\partial t} = \nabla \cdot (\kappa \nabla T) \quad \text{in } Q := \Omega \times (t_0, t_1), \quad (25)$$

$$\mathbf{n} \cdot \kappa \nabla T = \begin{cases} J(t) & \text{on } \Gamma_0 \times (t_0, t_1), \\ h(T^* - T) & \text{on } \Gamma_1 \times (t_0, t_1), \\ 0 & \text{on } \Gamma_2 \times (t_0, t_1), \end{cases} \quad (26)$$

$$T(x, t_0) = T_0(x) \quad \text{in } \Omega. \quad (27)$$

Here, $J(t)$ stands for the heat flux through the upper boundary Γ_0 of the module. At the lower boundary Γ_1 , a heat exchange with the cooling device takes place with h being the heat transition coefficient and T^* the temperature of the ambient medium.

The lateral boundary Γ_2 is assumed to be thermally insulated. Lastly, the functions ρ , c and κ denote the density, heat capacity and thermal conductivity which change discontinuously across the material interfaces.

The increase in temperature gives rise to heat stresses causing mechanical deformations \mathbf{u} that are described by the equilibrium equations of linear elasticity

$$\operatorname{div} \boldsymbol{\sigma}(\mathbf{u}) = \frac{\alpha(1-\nu)E}{(1+\nu)(1-2\nu)} \nabla(T - T_0) \quad \text{in } \Omega, \quad (28)$$

$$\mathbf{u} = 0 \text{ on } \Gamma_1, \quad \mathbf{n} \cdot \boldsymbol{\sigma}(\mathbf{u}) = 0 \quad \text{on } \Gamma \setminus \Gamma_1. \quad (29)$$

Here, $\boldsymbol{\sigma}(\mathbf{u})$ refers to the stress tensor

$$\boldsymbol{\sigma}(\mathbf{u}) = \frac{E}{1+\nu} \left[\mathcal{D}(\mathbf{u}) + \frac{\nu}{1-2\nu} \operatorname{tr} \mathcal{D}(\mathbf{u}) \mathbf{I} \right] \quad (30)$$

where $\mathcal{D}(\mathbf{u}) := \frac{1}{2}(\nabla \mathbf{u} + (\nabla \mathbf{u})^T)$ is the linearized strain tensor and E , ν stand for Young's modulus and Poisson's ratio, respectively. Note that α in (28) refers to the heat expansion coefficient. Again, the functions α , ν and E change discontinuously across material interfaces.

The numerical solution of the system of PDEs (22)–(24), (25)–(27) and (28)–(30) is treated in such a way that the drift diffusion equations (22)–(24) are decoupled in so far as they are taken care of in a preprocessing step by means of an adaptive mixed hybrid finite element approach (cf. [14, 15]). This gives rise to the Joule heat H_{Joule} and the heat flux $J(t)$ as the input data for the heat equation. The heat equation (25)–(27), implicitly discretized in time, and the elasticity equations (28)–(30) are solved by the mortar P1 element method as described in Sect. 2 based on a nonoverlapping decomposition of the computational domain as suggested by the sandwich-like structure of the IHV module (cf. Fig. 1).

On this basis, we have computed the distribution of the temperature T , the mechanical deformations \mathbf{u} , and the von Mises equivalence stresses $\sigma^{(E)} := \|\boldsymbol{\sigma}^{(D)}\|_F$ where $\boldsymbol{\sigma}^{(D)} := \boldsymbol{\sigma} - \frac{1}{3} \operatorname{tr} \boldsymbol{\sigma} \mathbf{I}$ is the deviatoric stress tensor and $\|\cdot\|_F$ refers to the Frobenius norm, i.e., $\|\boldsymbol{\sigma}^{(D)}\|_F := (\sum_{i,j=1}^3 (\sigma_{ij}^{(D)})^2)^{1/2}$.

Figures 2–5 represent visualizations of the temperature distribution T and the equivalence stresses $\sigma^{(E)}$ in the clipping planes corresponding to the upper and lower soldered joints (cf. Fig. 1). The grey scales range from high temperatures significantly above 100°C (white regions) to room temperature (black regions) and from high equivalence stresses in the range of several hundred MPa (white regions) to low equivalence stresses (black regions).

As expected, the temperature peaks occur below the copper blocks housing the IGBTs and power diodes. High values of the equivalence stresses can be observed in a string-like manner at the center of the upper soldered joint (cf. Fig. 4) whereas for the lower soldered joint the highest values are seen at the lateral boundary of the joint (cf. Fig. 5). This conforms very well to observed experimental data.

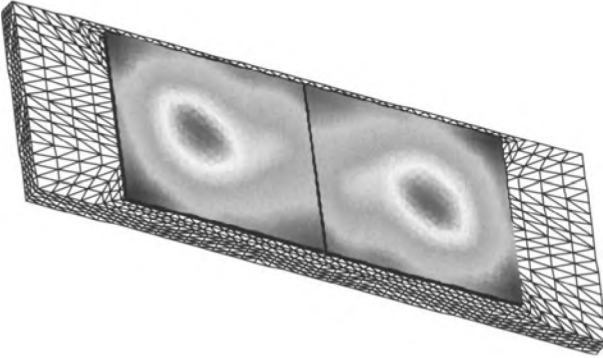


Fig. 2. Temperature distribution for the upper soldered joint

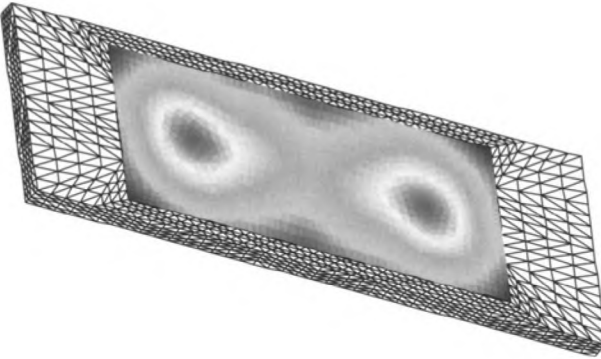


Fig. 3. Temperature distribution for the lower soldered joint

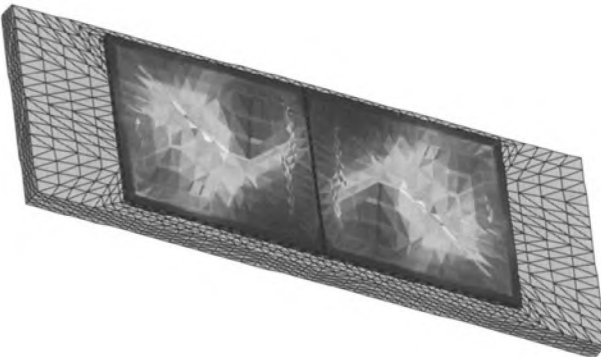


Fig. 4. Equivalence stresses for the upper soldered joint

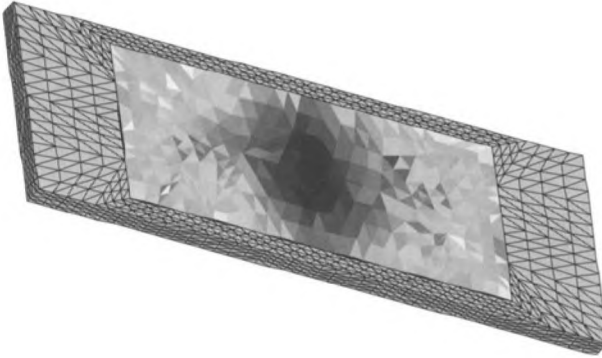


Fig. 5. Equivalence stresses for the lower soldered joint

4 Structural optimization of converter modules

As an application of the mortar edge element method we deal with the optimal layout and design of AC–DC converter modules that are based on the pulse width modulation technique and used as electric drives for high power electromotors.

Such a converter module consists of semiconductor devices (insulated gate bipolar transistors (IGBTs) and gate turn-off thyristors (GTOs)) serving as valves for the electric currents with switching times less than 100 ns. The IGBTs and GTOs are connected to each other and linked to the power source and the load by copper-made bus bars (cf. Fig. 6 (left)). The interconnecting bus bars are of a somewhat complex 3D geometric structure displaying several contacts where the semiconductor devices can be attached (cf. Fig. 6 (right)).

The problem is that, due to steep current ramps and the fast switching times, eddy currents are generated in the bus bars causing parasitic inductivities that lead to a significant power loss in the transmission. Therefore, the design objective is to minimize the parasitic inductivities. This can be done by placing holes in the

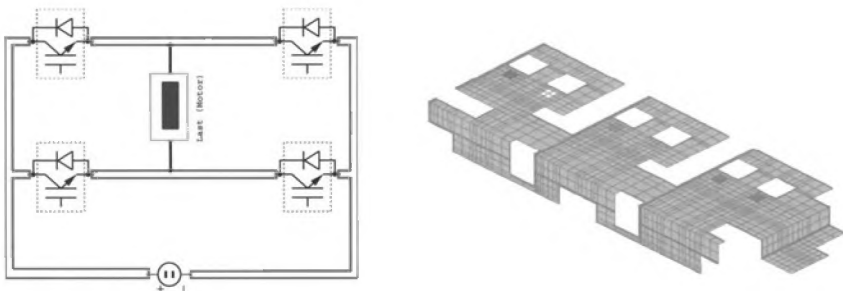


Fig. 6. Converter module (left) and bus bar (right)

material, typically in the vicinity of the contacts, since this essentially influences the distribution of the eddy currents within the interconnects.

From a mathematical point of view, the problem can be put into the frame of a topology-optimization problem subject to both equality and inequality constraints on the design parameters and state variables.

For simplicity, we restrict our considerations to the optimization of a single bus bar occupying a bounded domain Ω in \mathbf{R}^3 with N contacts $\Gamma_\nu \subset \partial\Omega$, $1 \leq \nu \leq N$.

The generation of the eddy currents can be described by the eddy current equations which we consider in their potential formulation by means of a scalar electric potential φ and a magnetic vector potential \mathbf{A} . This gives rise to a coupled system of PDEs:

$$\operatorname{div}(\sigma \mathbf{grad} \varphi) = 0 \quad \text{in } \Omega, \tag{31}$$

$$\mathbf{n} \cdot \sigma \mathbf{grad} \varphi = \begin{cases} -I_\nu(t) & \text{on } \Gamma_\nu, \\ 0 & \text{on } \Gamma \setminus \Gamma_\nu, \end{cases} \tag{32}$$

$$\sigma \frac{\partial \mathbf{A}}{\partial t} + \operatorname{curl} \mu \operatorname{curl} \mathbf{A} = \begin{cases} -\sigma \mathbf{grad} \varphi & \text{in } \Omega, \\ 0 & \text{in } \mathbf{R}^3 \setminus \bar{\Omega}, \end{cases} \tag{33}$$

the last with appropriate initial and boundary conditions.

Here, σ stands for the electric conductivity, μ refers to the magnetic permeability, and I_ν are the fluxes associated with the contacts Γ_ν satisfying $\sum_{\nu=1}^N I_\nu = 0$.

The total inductivity caused by the eddy currents is given by

$$L(\sigma, \varphi, \mathbf{A}) := \left(\sum_{\nu, \mu=1}^N \int_0^T |L_{\nu\mu}(t)|^2 dt \right)^{1/2}. \tag{34}$$

Here, $L_{\nu\mu}(t)$, $1 \leq \nu, \mu \leq N$, are the generalized transient inductivity coefficients

$$L_{\nu\mu}(t) := \sigma^{-1} \int_{\Omega} \mathbf{J}_\nu(x) \cdot \mathbf{S}(t) \mathbf{J}_\mu(x) dx,$$

where \mathbf{J}_ν refers to the current density generated by I_ν at port Γ_ν and $\mathbf{S}(\cdot)$ is the solution operator (semigroup) associated with the parabolic problem (33).

The form (34) of the objective functional suggests choosing the conductivity σ as the design parameter so that the design objective is to distribute the material in such a way that the total inductivity is minimized:

$$\inf_{\sigma, \varphi, \mathbf{A}} L(\sigma, \varphi, \mathbf{A}) \tag{35}$$

subject to the equality constraints

$$\varphi, \mathbf{A} \text{ satisfy (31)–(33),} \tag{36}$$

$$\int_{\Omega} \sigma dx = C, \tag{37}$$

$$\sigma_{\min} \leq \sigma \leq \sigma_{\max}, \tag{38}$$

where $0 < \sigma_{\min} \ll 1$ and σ_{\max} stands for the conductivity of copper. Note that σ_{\min} is chosen positive in order to preserve the ellipticity of the problem. In practice, the extreme values σ_{\min} and σ_{\max} are enforced by a simple isotropic method with penalization (SIMP) approach (for details see, e.g., [20, 21]).

The state equation (33) is discretized implicitly in time (backward Euler) and by a mortar edge element method in space using individual edge element discretizations of the interior and exterior problems, the exterior domain featuring an artificial boundary at a sufficiently large distance from the boundary of the interior domain. The elliptic boundary value problem (31), (32) is discretized by the lowest order nonconforming P1 elements with respect to the simplicial triangulation $\mathcal{T}_h^{(I)}$ of the interior domain. Note that a nonconforming approach has been chosen in order to avoid checkerboards in the design which typically occur for the lowest order conforming P1 elements. Lastly, the design parameter σ is discretized by elementwise constants.

Denoting the discrete design parameter by σ_h and the discrete state variables by $u_h = (\varphi_h, \mathbf{A}_h)^T$, we write the discretized state equations in the compact form

$$A_h(\sigma_h) = b_h \tag{39}$$

with the coefficient matrix $A_h(\sigma_h)$ and right-hand side b_h . Further, we refer to $L_h(\sigma_h, \varphi_h, \mathbf{A}_h)$ as the discretized objective functional.

Then, the discretized topology-optimization problem can be stated as follows:

$$\min_{\sigma_h, \varphi_h, \mathbf{A}_h} L_h(\sigma_h, \varphi_h, \mathbf{A}_h) \tag{40}$$

subject to the constraints

$$u_h = (\varphi_h, \mathbf{A}_h)^T \text{ satisfies (39),} \tag{41}$$

$$g_h(\sigma_h) = \sum_{i=1}^{m_h} |K_i| \sigma_h^{(i)} = C, \tag{42}$$

$$\sigma_{\min} \mathbf{e}_h \leq \sigma_h \leq \sigma_{\max} \mathbf{e}_h, \tag{43}$$

where $K_i \in \mathcal{T}_h^{(I)}$, $1 \leq i \leq m_h := \text{card } \mathcal{T}_h^{(I)}$, and $\mathbf{e}_h := (1, \dots, 1)^T$. The constrained optimization problem (40)–(43) is solved by an all-in-one approach featuring a primal-dual Newton interior-point method where the iterative solution of the discretized state equations is an integral part of the optimization routine. The interior-point aspect comes into effect by using parametrized logarithmic barrier functions

$$B_h^{(p)}(\sigma_h, \mathbf{u}_h) := L_h(\sigma_h, \varphi_h, \mathbf{u}_h) - p[\log(\sigma_h - \sigma_{\min} \mathbf{e}_h) + \log(\sigma_{\max} \mathbf{e}_h - \sigma_h)],$$

whereas the primal-dual aspect is taken care of by Lagrange multipliers λ_h, η_h for coupling the equality constraints (41),(42). We are thus led to the saddle point problem

$$\min_{\sigma_h, \mathbf{u}_h} \max_{\lambda_h, \eta_h} \mathcal{L}_h^{(p)}(\sigma_h, \mathbf{u}_h, \lambda_h, \eta_h) \tag{44}$$

where the Lagrange functional $\mathcal{L}_h^{(p)}$ is given by

$$\mathcal{L}_h^{(p)}(\sigma_h, \mathbf{u}_h, \boldsymbol{\lambda}_h, \eta_h) := B_h^{(p)}(\sigma_h, \mathbf{u}_h) + \boldsymbol{\lambda}_h^T (A_h(\sigma_h) \mathbf{u}_h - b_h) + \eta_h (g_h(\sigma_h) - C).$$

For the numerical solution of (44) we use simultaneous sequential quadratic programming (SQP) by applying Newton's method to the Karush–Kuhn–Tucker (KKT) conditions associated with (44). In each Newton step, the linear algebraic system for the Newton increments is solved iteratively by right transforming iterations based on a null space decomposition of the condensed primal-dual Hessian. It is at this stage that the mortar edge element techniques described in Sect. 2 are invoked. The new Newton iterates are determined by a line search where the step-lengths are tested using a hierarchy of two merit functions combined with a watchdog strategy (we refer to [20, 21] for details).

Computed local minima of the objective functional give rise to designs that are usually postprocessed in order to take further technological constraints (e.g., the shape of the holes) into account. For such a postprocessed design, Fig. 7 shows the distribution of the electric currents while Fig. 8 displays the magnetic induction $\mathbf{B} = \mathbf{curl} \mathbf{A}$ in the vicinity of two contacts illustrating the effect of the holes on the generated electromagnetic fields.

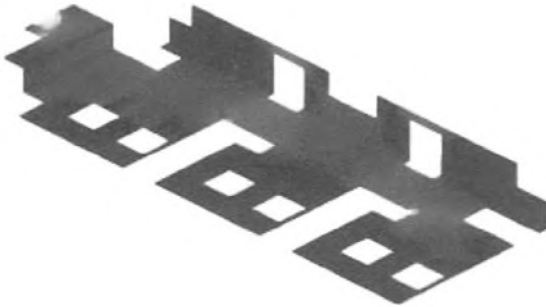


Fig. 7. Distribution of the electric currents in an optimized bus bar

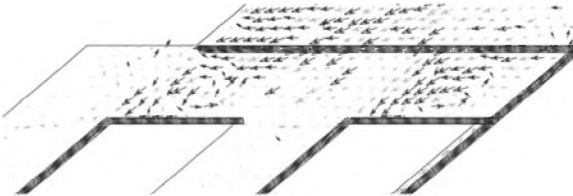


Fig. 8. Distribution of the magnetic induction in an optimized bus bar

Acknowledgements. This work has been supported by the German National Science Foundation (DFG) within the Sonderforschungsbereich 438 as well as by the Grants No. HO877/4-1, No. HO877/5-1, by the Federal Ministry for Education and Research (BMBF) under Grants No. 03HO7AU1, No. 03HOM3A1, and by the Bavarian Consortium for High Performance Scientific Computing (FORT WIHR).

References

- [1] Achdou, Y., Kuznetsov, Yu.A. (1995): Substructuring preconditioners for finite element methods on nonmatching grids. *East–West J. Numer. Math.* **3**, 1–28
- [2] Achdou, Y., Maday, Y., Widlund, O.B. (1996): Méthode itérative de sous-structuration pour les éléments avec joints. *C.R. Acad. Sci. Paris Sér. I Math.* **322**, 185–190
- [3] Beck, R., Deuffhard, P., Hiptmair, R., Hoppe, R.H.W., Wohlmuth, B. (1999): Adaptive multilevel methods for edge element discretizations of Maxwell’s equations. *Surveys Math. Indust.* **8**, 271–312
- [4] Beck, R., Hiptmair, R., Hoppe, R.H.W., Wohlmuth, B. (2000): Residual based a posteriori error estimators for eddy current computation. *M2AN Math. Model. Numer. Anal.* **34**, 159–182
- [5] Ben Belgacem, F., Maday, Y. (1997): The mortar element method for three-dimensional finite elements. *RAIRO Math. Modél. Anal. Numer.* **31**, 289–302
- [6] Ben Belgacem, F., Buffa, A., Maday, Y. (2001): The mortar finite element method for 3D Maxwell equations: first results. *SIAM J. Numer. Anal.* **39**, 880–901
- [7] Bernardi, Chr., Maday, Y., Patera, A. (1993): Domain decomposition by the mortar element method. In: Kaper, H.G. et al. (eds.): *Asymptotic and numerical methods for partial differential equations with critical parameters*. Kluwer, Dordrecht, pp. 269–286
- [8] Bernardi, Chr., Maday, Y., Patera, A. (1994): A new nonconforming approach to domain decomposition: the mortar element method. In: Brézis, H., Lions, J.-L. (eds.): *Nonlinear partial differential equations and their applications*. Collège de France Seminar. Vol. XI. Longman, Harlow, pp. 13–51
- [9] Böhm, P., Gerstenmaier, Y.C., Hoppe, R.H.W., Iliash, Y., Mazurkevitch, G., Wachutka, G. (2002): Modeling and simulation of electrothermomechanical coupling phenomena in high power electronics. In: Breuer, M. et al. (eds.): *High performance scientific and engineering computing*. (Lecture Notes in Computational Science and Engineering, vol. 21). Springer, Berlin, pp. 393–400
- [10] Braess, D., Dahmen, W. (1998): Stability estimates of the mortar finite element method for 3-dimensional problems. *East–West J. Numer. Math.* **6**, 249–263
- [11] Brezzi, F., Marini, D. (2001): Error estimates for the three-field formulation with bubble stabilization. *Math. Comp.* **70**, 911–934
- [12] Engelmann, B., Hoppe, R.H.W., Iliash, Y., Kuznetsov, Y., Vassilevski, Y., Wohlmuth, B. (2000): Adaptive finite element methods for domain decomposition on nonmatching grids. In: Bjørstad, P., Luskin, M. (eds.): *Parallel solution of partial differential equations*. (The IMA Volumes in Mathematics and its Applications, vol. 120). Springer, Berlin, pp. 57–83
- [13] Hiptmair, R. (1999): Multigrid method for Maxwell’s equations. *SIAM J. Numer. Anal.* **36**, 204–225
- [14] Hiptmair, R., Hoppe, R.H.W. (1994): Mixed finite element discretization of continuity equations arising in semiconductor simulation. In: Bank, R.E. et al. (eds.): *Mathematical*

- modeling and simulation of electrical circuits and semiconductor devices. Birkhäuser, Basel, pp. 197–217
- [15] Hiptmair, R., Hoppe, R.H.W., Wohlmuth, B. (1995): Coupling problems in microelectronic device simulation. In: Hackbusch, W., Wittum, G. (eds.): Numerical treatment of coupled systems. (Notes on Numerical Fluid Mechanics, vol. 51) Vieweg, Wiesbaden, pp. 86–95
- [16] Hoppe, R. H.W. (1999): Mortar edge elements in \mathbf{R}^3 . East–West J. Numer. Anal. **7**, 159–173
- [17] Hoppe, R.H.W. (2001): Efficient numerical solution techniques in electromagnetic field computation. In: 2nd European conference on computational mechanics. Institute of Computer Methods in Civil Engineering, Cracow University of Technology, Cracow. CD-Rom
- [18] Hoppe, R.H.W., Iliash, Y., Kuznetsov, Y., Vassilevski, Y., Wohlmuth, B. (1998): Analysis and parallel implementation of adaptive mortar element methods. East–West J. Numer. Math. **6**, 223–248
- [19] Hoppe, R.H.W., Iliash, Y., Mazurkevitch, G. (2000): Domain decomposition methods in the design of high power electronic devices. In: Sändig, A.-M. et al. (eds.): Multifield problems. Springer, Berlin, pp. 169–182
- [20] Hoppe, R.H.W., Petrova, S., Schulz, V. (2002): 3D structural optimization in electromagnetics. In: Debit, N. et al. (eds.): Proceedings of the 13th international conference on domain decomposition methods in Lyon, France. CIMNE, Barcelona, pp. 469–476
- [21] Hoppe, R.H.W., Petrova, S., Schulz, V. (2002): Primal-dual Newton-type interior-point method for topology optimization. J. Optim. Theory Appl. **114**, 545–571
- [22] Kuznetsov, Yu.A., Wheeler, M.F. (1995): Optimal order substructuring preconditioners for mixed finite element methods on nonmatching grids. East–West J. Numer. Math. **3**, 127–143
- [23] Markovich, P., Ringhofer, Chr., Schmeiser, Chr. (1990): Semiconductor equations. Springer, Vienna
- [24] Nédélec, J. (1980): Mixed finite elements in \mathbf{R}^3 . Numer. Math. **35**, 315–341
- [25] Rapetti, F. (2000): Approximation des equations de la magnetodynamique en domaine tournant par la méthode des elements avec joints. Ph.D. thesis, Université Pierre et Marie Curie – Paris 6, Paris
- [26] Selberherr, S. (1984): Analysis and simulation of semiconductor devices. Springer, Berlin
- [27] Wachutka, G. (1999): The art of modeling coupled-field effects in microdevices and microsystems. In: Technical proceedings 1999 international conference on modeling and simulation of microsystems. Applied Computational Research Society, Cambridge, MA, pp. 14–19
- [28] Wohlmuth, B. (2001): Discretization methods and iterative solvers based on domain decomposition. (Lecture Notes in Computational Science and Engineering, vol. 17). Springer, Berlin